2015 IEEE International Conference on Robotics and Automation (ICRA)
Washington State Convention Center
Seattle, Washington, May 26-30, 2015

Photoacoustic Image Guidance for Robot-Assisted Skull Base Surgery

Sungmin Kim, Hyun Jae Kang, Alexis Cheng, Muyinatu A. Lediju Bell, Emad Boctor and Peter Kazanzides

Abstract— **We are investigating the use of photoacoustic (PA) imaging to detect critical structures, such as the carotid artery, that may be located behind the bone being drilled during robot-assisted endonasal transsphenoidal surgery. In this system, the laser is mounted on the drill (via an optical fiber) and the 2D ultrasound (US) probe is placed elsewhere on the skull. Both the drill and the US probe are tracked relative to the patient reference frame. PA imaging provides two advantages compared to conventional B-mode US: (1) the laser penetrates thin layers of bone, and (2) the PA image displays targets that are in the laser path. Thus, the laser can be used to (non-invasively) extend the drill axis, thereby enabling reliable detection of critical structures that may reside in the drill path. This setup creates a challenging alignment problem, however, because the US probe must be placed so that its image plane intersects the laser line in the neighborhood of the target anatomy (as estimated from preoperative images). This paper reports on a navigation system developed to assist with this task, and the results of phantom experiments that demonstrate that a critical structure can be detected with an accuracy of approximately 1 mm relative to the drill tip.**

I. Introduction

Removing pituitary tumors via an endoscopic transnasal transsphenoidal approach is generally effective, but can result in serious complications such as damage to the carotid artery [1]. While endoscopes or microscopes provide visualization of anatomical structures, this visualization is limited to surface features, which are not always distinct enough to provide accurate localization. In particular, an endoscope cannot detect whether an artery is located behind the bone being drilled. While a navigation system can be used to localize surgical instruments with respect to sub-surface anatomy, it suffers from inaccuracies in the registration between the preoperative image and the intraoperative coordinate frame.

This motivates the development of an intraoperative imaging modality that can directly detect critical structures, such as the carotid artery, even when located behind the skull bone. Ideally, this imaging modality should provide real-time feedback (during drilling, if possible), not introduce additional risk to the patient (e.g., through ionizing radiation), and should be feasible to use in a conventional operating room. These requirements eliminate x-ray and CT, due to the radiation, and MRI because it is not widely available in operating rooms and imposes severe environmental constraints (i.e., no electromagnetic fields or ferro-magnetic materials). Optical coherence tomography (OCT) is one possibility, but its imaging depth is typically limited to a few millimeters. Ultrasound is a promising candidate because it is safe, inexpensive, and widely available. But, it is difficult to obtain high-quality images through bone due to sound attenuation and scattering.

We are exploring the use of photoacoustic (PA) imaging to provide real-time monitoring of the drilling process. The physical basis for PA imaging is the photoacoustic effect; it refers to the generation of acoustic waves by the absorption of electromagnetic energy, such as the light from a pulsed laser beam. The oxygen saturation and concentration of hemoglobin is sensitive to the optical excitation and absorption (at the appropriate wavelengths), allowing the detection of blood vessels. We therefore propose to attach a pulsed laser to the drill, which can be hand-held or robotically controlled, and to place an ultrasound probe (receiver) elsewhere on the skull surface to detect the generated acoustic waves. Our previous study [2] demonstrated the feasibility of using PA imaging to detect anatomic targets using this geometric arrangement of laser and ultrasound probe, in cases where conventional ultrasound failed.

It can be difficult, however, to align the ultrasound probe so that its imaging plane intersects the laser beam near the suspected location of the anatomical feature of interest (target). This paper presents an image-guided assistant system to guide the placement of the tracked ultrasound probe, based on the location of the tracked laser and the anatomical target. We perform phantom experiments to demonstrate that this approach can potentially detect targets with an accuracy of about 1 mm. Grunert et al [3] surveyed the neurosurgical literature and reported ranges of 0.2-3.0mm for registration error and 0.6-10.0mm for application error, which also includes errors due to anatomical changes during surgery. For skull base surgery, application errors of 0.91-2.44mm were reported in a cadaver study [4]. Because PA imaging provides real-time measurement of anatomy, our results suggest that it is possible to obtain an application accuracy that is well within this range.

II. System Overview

The main components of the system are a surgical drill, pulsed laser, ultrasound probe and scanner, and navigation (optical tracking) system, as shown in Fig. 1. This figure also includes a phantom (patient), created from a CAD model, to provide ground-truth measurements for the reported experiments. The navigation system determines the spatial relationships between the drill (and laser beam), ultrasound probe, and patient. Ultimately, we expect the drill to be mounted on the end of a robot, which is either teleoperated or cooperatively-controlled by the surgeon. The ultrasound

Authors are with the Department of Computer Science, Johns Hopkins University, Baltimore, MD 21218, USA. Sungmin Kim can be contacted at sungminkim@jhu.edu.

probe could be held by a second robot or by a passive arm. The registration between the phantom coordinate system and the (optically-tracked) dynamic reference base (DRB) is obtained by using a tracked pointer to touch fiducials on the phantom, followed by a paired-point registration between these measured points and the coordinates of the points in the CAD model of the phantom (for a patient, a CT scan would be used instead of a CAD model). The transformation between the (optically-tracked) marker frame on the US probe and the US image plane is obtained by a calibration method that uses an active point phantom [5], which is a variant of the method described by Guo et al. [6]. The offset (translation) between the (optically-tracked) marker frame on the tool (drill) and the tool tip is obtained by a standard pivot calibration method. The laser line is calibrated with respect to the tool marker frame using the method described below (Tracking module).

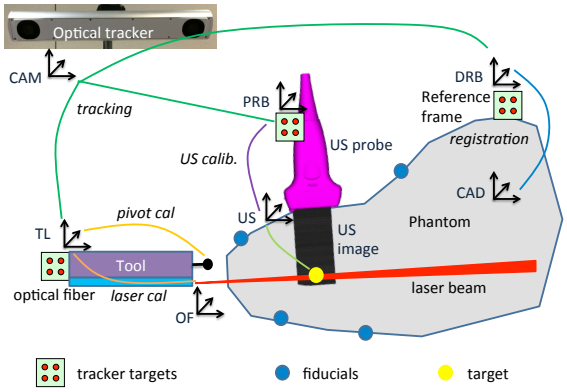

Fig. 1. Major components, coordinate frames and transformations. Text in italics indicates how transformations are obtained.

The transformation map shown in Fig. 1 supports three methods for computing the target with respect to the reference frame, P_{DRB}, where ${}^{B}T_{A}$ denotes the transformation *from* coordinate frame A *to* coordinate frame B and P_C is the target measured with respect to coordinate frame C:

1) The target point (in CAD model) can be transformed to the reference frame using the registration:
$P_{DRB} = {}^{DRB}T_{CAD}\ P_{CAD}$
2) If the target is visible in the PA image, it can be transformed from US image coordinates to the reference frame using the US probe calibration and the tracker measurements of the marker frames attached to the US probe and DRB:
$P_{DRB} = {}^{CAM}T_{DRB}^{-1}\ {}^{CAM}T_{PRB}\ {}^{PRB}T_{US}\ P_{US}$
3) If the target is visible in the PA image, we can compute its position from the intersection of the laser line with the US image plane:
$P_{DRB} = {}^{CAM}T_{DRB}^{-1}\ {}^{CAM}T_{TL}\ {}^{TL}T_{OF}\ P_{OF}$
where P_{OF} is the intersection point expressed in the optical fiber (OF) coordinate system.

In our experiments, the first method is used as the "ground truth". In a surgical scenario, this option may not be available if the critical structure (e.g., carotid artery) is not directly visible in the CT image. The second method is the most obvious approach, but we propose the third method because it is less dependent on accurate measurements from PA imaging. It does depend on accurate calibration of the laser line, which is easier to guarantee if the optical fiber is integrated with the tool. In the best case, if the laser can itself be the tool (i.e., if the laser is used for cutting), there would be zero error in the calibration. This approach essentially discards the position of the target in the PA image (i.e., it only cares whether or not the target is visible). One issue, however, is that this method is affected by divergence of the laser beam, which can be significant for an uncollimated fiber. But, this effect can be mitigated by sweeping the laser across the target and identifying the edges.

The software architecture consists of the Tracking module, Imaging module for B-mode or photoacoustic imaging, and the Photoacoustic Navigation module, as shown in Fig. 2.

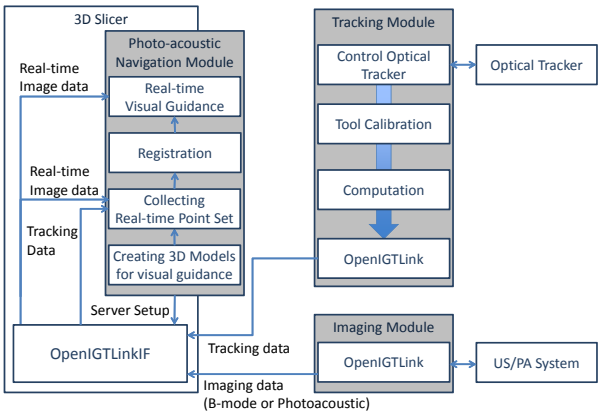

Fig. 2. System Overview: Assistant System for Photoacoustic Imaging

The **Tracking** module acquires and processes data from an optical tracker, handles tool calibration, and sends the tracking information to the Photoacoustic Navigation module. It is implemented in C++ using the *cisst* libraries and the Surgical Assistant Workstation (SAW) [7], which are open source software packages designed to ease the development of computer-assisted intervention systems. In particular, SAW includes components that interface to different tracking systems, including the Atracsys tracker (Atracsys LLC, Switzerland), used for the experiments reported here.

The Tracking module is designed to track the position of three marker frames, attached to the laser, the ultrasound probe, and the patient. The patient-attached frame serves as the dynamic reference base (DRB); as in a typical navigation setup, this enables the system to track the laser and probe with respect to the DRB, thereby achieving robustness against motion of the patient or tracking camera. The Tracking module also includes methods for tool calibration. The tool calibration employs a non-contact pivot calibration method where a visible laser beam (instead of the laser used for PA imaging) is directed to intersect a physical point in the workspace from different orientations.

The **Photoacoustic Navigation** module is a plugin module, written in Python, that is integrated with 3D Slicer [8] and provides visual guidance using the data from the Tracking

module. While it would have been possible to combine all functionality into a single module within 3D Slicer, for convenience we implemented them as two separate programs and used the OpenIGTLink network interface [9] for data exchange between the programs.

The Photoacoustic Navigation module includes 3D models of the ultrasound probe, laser tip, virtual laser path, and real-time ultrasound image plane. The probe is represented by a 3D CAD model of the ultrasound transducer and the laser tip is represented by a standard Slicer locator probe (see Fig. 3). The real-time ultrasound image plane shows real-time images received from the Imaging module and the virtual laser path is represented by a cylinder, as shown in Fig. 3.

The **Imaging** module has two implementations, one for B-mode ultrasound and one for photoacoustic (PA) imaging, and is installed on the ultrasound scanner and PA imaging system, respectively. It is implemented in C++ using the MUSiiC toolkit [10], [11] and can provide real-time B-mode or PA ultrasound images via OpenIGTLink. Although our proposed system relies exclusively on PA imaging, we use B-mode imaging for some of the validation experiments.

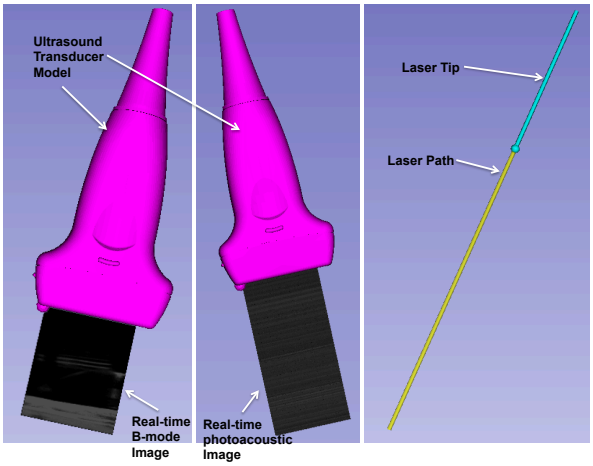

Fig. 3. Left: ultrasound probe model and real-time ultrasound images; Right: laser tip and virtual laser path

III. Experiments

A. Phantom

We designed and built a phantom, using a 3D printing machine, to evaluate the accuracy of our system (Fig. 4). The phantom contains 5 square pillars of different heights, each used as a ground-truth landmark. The top of each pillar has a hemi-spherical concavity to facilitate registration and to place spherical rubber targets for the photoacoustic imaging. The phantom is 60 x 25 x 25 mm and is fixed inside a plastic container that is 100 x 60 x 100 mm. The dynamic reference base (DRB) is fixed on the surface of the plastic container. During the experiments, the phantom was filled with water for ultrasound and photoacoustic imaging. After the registration procedure and experiment with ultrasound images, two spherical rubber targets (2.3 mm diameter) were fixed atop two of the pillars, which had a 10 mm height difference. The navigation assistant used the 3D CAD model, in STL format, rather than a CT scan. The model was displayed in the 3D view of 3D Slicer and used for the registration. Note that this phantom does not contain bone, so it enabled us to perform experiments with both B-mode ultrasound and PA imaging.

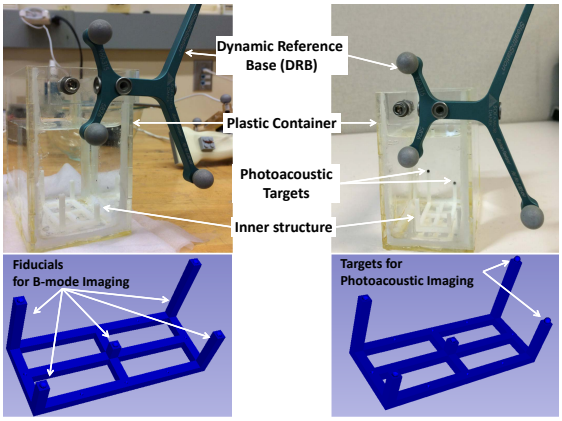

Fig. 4. Phantom embedded with inner structure for B-mode imaging (top left) and the CAD model of the inner structure (bottom left), and the phantom embedded with additional spherical rubber targets (top right) and the CAD model of the inner structure and two spherical targets (bottom right).

B. B-Mode Ultrasound and Photoacoustic Imaging

A SonixTouch ultrasound scanner, with an Ultrasonix L14-5W/38 linear transducer, was used for the experiments. This transducer has a 5-14 MHz bandwidth. For the photoacoustic imaging, a 1 mm core diameter optical fiber with a 0.37 mm numerical aperture was coupled to a 1064 nm Nd:YAG laser.

Image data was obtained from the Imaging module with OpenIGTLink network interfaces. The ultrasound and photoacoustic images were displayed with the ultrasound transducer model, laser tip model and virtual laser path model on the 3D view of 3D Slicer in real-time.

C. Experimental Setup

Marker frames were attached to the ultrasound transducer (probe), laser tip holder, and phantom, as illustrated in Fig. 1. To hold and move the ultrasound transducer, a UR5 robotic arm (Universal Robots Inc., Odense, Denmark) was applied to reduce tremor of the transducer during image acquisition and to move precisely.

The phantom was placed on the table beside the laser system for photoacoustic imaging, and the optical fiber was fixed on the holder. The tracking camera was placed so that its field of view encompassed the entire scene of the experimental setup, as shown in Fig. 5. The Tracking and Photoacoustic Navigation modules were installed on a laptop near the experimental setup.

In addition, after the optical fiber was fixed on the laser tip holder, some calibration procedures were conducted. First, the tool tip offset and the direction matrix of the tool tip were estimated using manual procedures. Then, the accuracy of the tool tip offset was confirmed via a standard pivot calibration method. Finally, the direction of the laser path was confirmed by using a non-contact pivot calibration method, where the

laser spot was aimed at a fixed point in the workspace from different tool orientations.

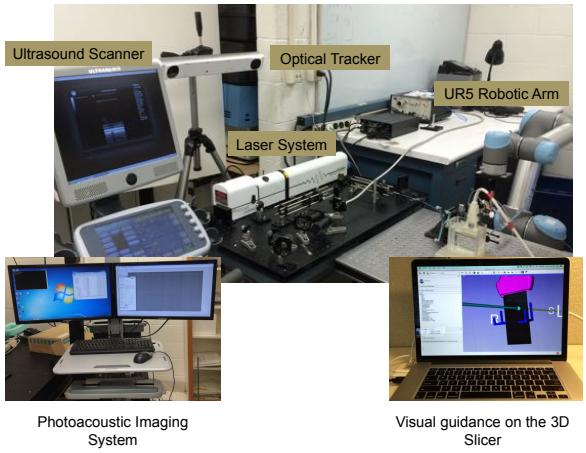

Fig. 5. Experimental setup for photoacoustic imaging assistant system

D. Experimental Procedures

We conducted two different experiments to evaluate the accuracy of our assistant system for photoacoustic imaging. The first experiment uses B-mode imaging to evaluate the navigation accuracy of our experimental setup. The second experiment evaluates the accuracy of real-time measurement with the photoacoustic image, using the registered CAD model as the ground-truth. We also collected B-mode images in this setup for comparison; although B-mode imaging is not feasible for the intended skull base surgery application (due to the bone), it may be applicable to procedures elsewhere in the body.

After setting up all devices and applications, and before fixing the optical fiber to the optical fiber holder, we registered the tracking system to the preoperative 3D CAD model. This registration was accomplished by touching the fiducials of the phantom with a tracked pointer (i.e., the optical fiber holder), and performing a paired-point registration between the fiducial positions measured by the tracker and their corresponding positions in the 3D CAD model. Because the dynamic reference base was attached to the phantom, it is not necessary to repeat the registration procedures even if the phantom or tracking camera is repositioned.

For the first experiment, the ultrasound transducer was placed by an expert using the robotic arm for B-mode imaging, and then the positions of the pillars were compared with the B-mode image and 3D CAD model in the 3D view of 3D Slicer (Fig. 6). This procedure was repeated for the 5 pillars.

For the second experiment, the ultrasound transducer and laser tip were placed using the visual guidance information of the 3D view of 3D Slicer (Fig. 7). Subsequently, photoacoustic and B-mode ultrasound images were acquired. These procedures were performed for the two spherical rubber targets.

IV. Results

For the first experiment, we acquired B-mode images after positioning the ultrasound transducer to locate each of the

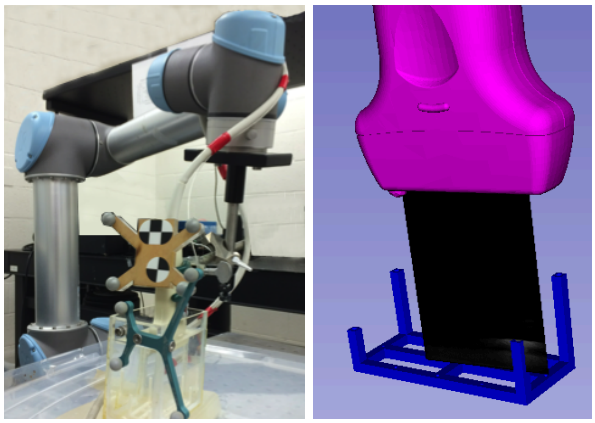

Fig. 6. Positioning ultrasound transducer for B-mode imaging (left), and 3D visualization on 3D Slicer (right)

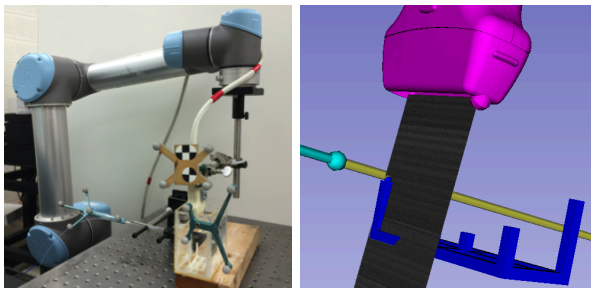

Fig. 7. Positioning ultrasound transducer and laser tip for photoacoustic imaging (left), and 3D visualization on 3D Slicer (right)

five pillars on the phantom. Annotated screenshots of the Photoacoustic Assistant module (e.g., the 3D view from 3D Slicer) are shown in Fig. 8-top. Here, the error between the B-mode image and the phantom model is visually apparent. We computed the distance errors between the pillars identified in the B-mode images and the corresponding positions in the 3D CAD model. This computation was performed in the DRB reference frame. Thus, the pillar positions in the B-mode images required the following three transformations: (1) ultrasound probe calibration, (2) ultrasound marker frame to tracking camera, and (3) tracking camera to DRB marker frame. The ground-truth positions (from the 3D CAD model) were transformed using the registration between the CAD model and the DRB, and thus are subject to registration error; however, we believe this to be small due to the use of multiple fiducials and the high accuracy of the CAD model. The results (Table I) show a mean accuracy of 0.97 mm for the overall system, which verifies the accuracy of the US probe calibration, tracking system, and registration between CAD model and DRB. Note that this experiment does not verify the accuracy of the tool tip or laser line calibration, since these do not affect the B-mode images.

For each target in the second experiment, the ultrasound transducer and laser tip were positioned with visual guidance of the photoacoustic assistant system and PA and B-mode images were acquired (see Fig. 9). The bottom row of Fig. 8 presents the visual guidance interface with real-time PA images and models of the laser tip and laser path. This figure shows that the intersection of virtual laser path with

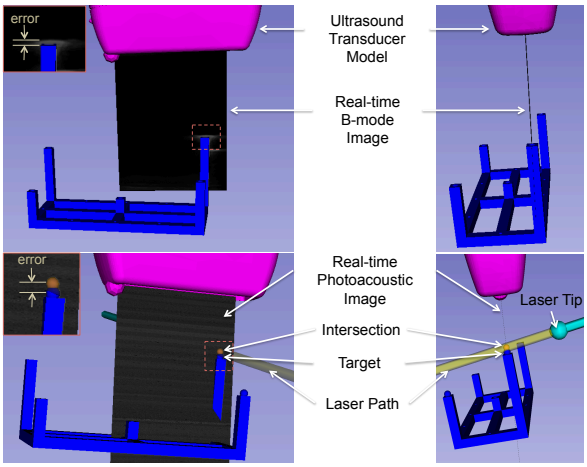

Fig. 8. Photoacoustic Assistant module: screenshots for experiment with B-mode imaging (top row) and experiment with photoacoustic imaging (bottom row).

TABLE I
DISTANCE BETWEEN GROUND TRUTH AND B-MODE IMAGE

US Target #	Error, mm
1	1.631
2	0.865
3	0.902
4	0.866
5	0.563
Mean	0.966

the real-time PA image plane are close to the targets of the phantom, though small errors are evident; the intersection and the target are represented by red and blue balls, respectively. The B-mode images were acquired to give additional insight into the content of the PA images, as shown in Fig. 9, and are not used in the subsequent data analysis.

We compute the translation vector from the laser tip to the target position using the three methods proposed in Section II (technically, we want the vector from the tool tip to the target, but for these experiments the tool tip is identical to the laser tip; in general, there would be a known offset). For more intuitive understanding, we express the results in the coordinate frame of the US image, where the US image plane is approximately orthogonal to the laser line. Figure 10 shows the measurements expressed in the US image plane (i.e., lateral and axial directions), where the *Intersection (Navigation)* and *Photoacoustic* data correspond to Methods 3 and 2, respectively, in Section II. Relative to each other, the methods produce similar results in the lateral direction, with a larger discrepancy in the axial direction. The elevational error (i.e., perpendicular to the image plane) is identical for the two methods because they are both restricted to the US image plane.

Table II compares each measurement to the ground-truth, obtained by applying the registration transformation to the target positions from the CAD model (Method 1 in Section II).

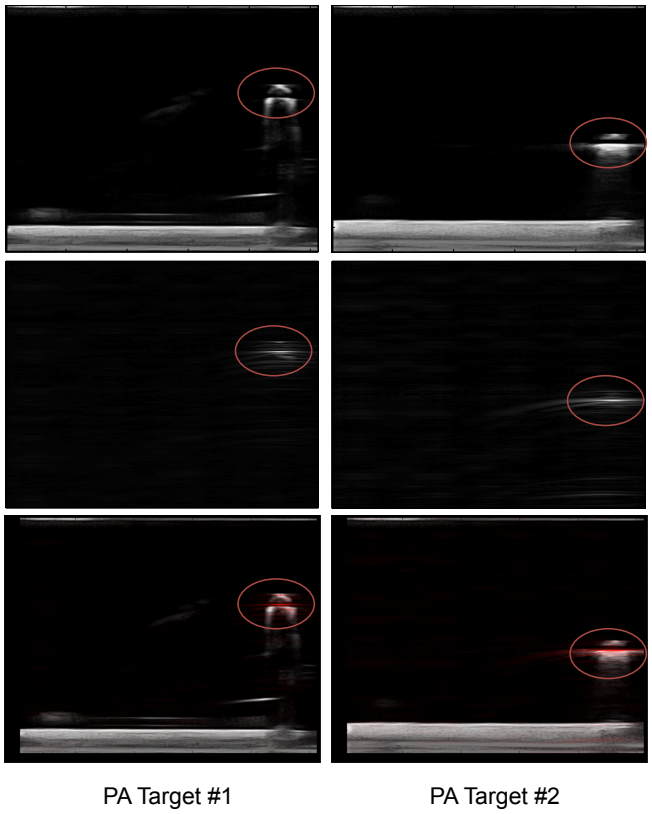

Fig. 9. Photoacoustic imaging results for two targets: B-mode images (top), photoacoustic images (middle), and overlaid images (bottom); red circles indicate target.

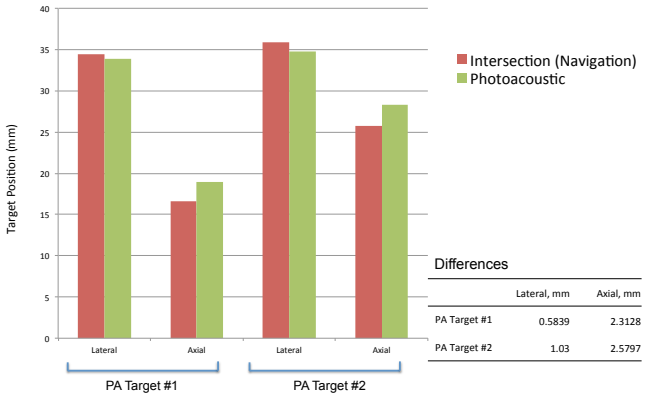

Fig. 10. Comparison of target positions measured in US image plane for Intersection with Navigation (Method 3) and Photoacoustic (Method 2)

V. DISCUSSION AND CONCLUSIONS

This study focused on the development and experimental evaluation of a navigation system to guide the placement of a laser and/or ultrasound probe to obtain photoacoustic images during endonasal skull base drilling. The ultimate goal is to use the photoacoustic images to provide real-time measurement of the location of critical structures, such as the carotid artery, with respect to the drill tip. In one envisioned scenario, the laser and drill are mounted on a robot system which can use this information to dynamically construct or adjust virtual fixtures to protect the critical anatomy. In this case, the navigation system would primarily

TABLE II

ERROR IN MEASURED TARGET POSITION FOR INTERSECTION WITH NAVIGATION (METHOD 3) AND PHOTOACOUSTIC (METHOD 2), COMPARED TO GROUND-TRUTH (METHOD 1). UNITS ARE MM.

PA	Intersection (Nav.)		Photoacoustic		(Both)
Target #	Lateral	Axial	Lateral	Axial	Elevational
1	0.12	0.32	0.7	-1.99	0.079
2	-0.92	-0.16	0.11	-2.74	1.332

be used to position the ultrasound probe, though it could also provide guidance to the surgeon (or robot) to make minor adjustments to the drill (laser) orientation to gain additional image information.

The experiments showed the feasibility of the developed navigation system to provide visual guidance to the user to align the laser and probe to obtain a PA image of a desired target. Here, the target is identified on a 3D CAD model, which is registered to the intraoperative (tracker) coordinate system to provide a ground-truth measurement. The results in Table II indicate that the mean error of the real-time measurement of the distance between the laser tip and the target is less than 1 mm when the proposed method (Intersection/Navigation) is used; this method relies on the accuracy of the laser line calibration with respect to the tool and only uses the tracked US probe to determine the distance from the tip to the image plane. The US image is primarily used as a binary flag to indicate whether or not the target is in the path of the laser. In reality, the situation is more complex due to the use of an uncollimated fiber, which causes significant divergence of the laser beam. The fiber used in these experiments has a numerical aperture of 0.37, which corresponds to a half-angle of approximately 16 degrees in water. At the fiber-to-target distances used in these experiments ($\approx$17 mm for PA Target #1 and $\approx$20 mm for PA Target #2), the initial 1 mm laser beam diameter diverges to diameters of $\approx$10.75 mm and $\approx$12.47 mm, respectively. Thus, the low errors in the lateral and axial directions shown in Table II for the Intersection (Nav.) measurement actually reflect good accuracy in the navigation system, which enabled the user to align the laser beam with the target. In reality, disturbing the beam by several millimeters in either direction (lateral or axial) would produce different measurements of the target position, even though the target obviously has not moved. In preliminary tests, we have determined that this effect can be mitigated by sweeping the laser beam back and forth around the target, in order to determine the true center of the target. This is the subject of current research efforts.

On the other hand, the relatively large error in the axial direction for the photoacoustic method may be due to several other factors, since this measurement is affected by errors in the probe calibration and tracking system, as well as by physical phenomenon such as a system bulk delay offset [12], which is the time difference between the start of a normal transmit event and actual laser firing time. Assuming the speed of sound in water is 1460 m/s, if the system bulk delay is 2 μs, we would expect an offset of 2.92 mm, which is comparable to the measured offsets in Table II.

Finally, we hope to apply this system to an environment that more realistically mimics endoscopic transnasal transsphenoidal approaches. For those experiments, the phantom should be modified to place real bone between the laser tip and target and the ultrasound transducer and target, as previously done in [2]. In this case, we hope to be able to obtain a photoacoustic signal from both the target and the bone adjacent to the laser tip. If so, we can position the US probe so that the image captures both measurements, enabling us to directly measure the distance between the tool tip (assuming it is in contact with the bone, e.g., during drilling) and the target. This would remove any dependency on the tracking accuracy of the US probe. If, however, we do not obtain a photoacoustic signal from the bone, the experiments reported in this paper indicate that we could still achieve accuracy on the order of 1 mm.

VI. ACKNOWLEDGMENTS

This work was supported by NSF NRI 1208540. M.A. Lediju Bell is a recipient of the UNCF-Merck and Ford Foundation Postdoctoral Fellowships.

REFERENCES

[1] P. Cappabianca, L. M. Cavallo, A. Colao, and E. de Divitiis, "Surgical complications associated with the endoscopic endonasal transsphenoidal approach for pituitary adenomas," *Journal of Neurosurgery*, vol. 97, no. 2, pp. 293–298, Aug 2002.

[2] M. A. Lediju Bell, A. K. Ostrowski, P. Kazanzides, and E. Boctor, "Feasibility of transcranial photoacoustic imaging for interventional guidance of endonasal surgeries," in *SPIE Photonics West*, vol. 8943, Feb 2014.

[3] P. Grunert, K. Darabi, J. Espinosa, and R. Filippi, "Computer-aided navigation in neurosurgery," *Neurosurgical Review*, vol. 26, no. 2, pp. 73–99, May 2003.

[4] F. D. Vrionis, K. T. Foley, J. H. Robertson, and J. J. Shea, "Use of cranial surface anatomic fiducials for interactive image-guided navigation in the temporal bone: A cadaveric study," *Neurosurgery*, vol. 40, no. 4, pp. 755–764, April 1997.

[5] A. Cheng, X. Guo, R. Etienne-Cummings, and E. Boctor, "Active point out-of-plane ultrasound calibration," in *SPIE Medical Imaging*, vol. 9415, Feb 2015.

[6] X. Guo, A. Cheng, H. K. Zhang, H. J. Kang, R. Etienne-Cummings, and E. Boctor, "Active echo: A new paradigm for ultrasound calibration," in *MICCAI*, 2014, pp. 397–404.

[7] P. Kazanzides, S. DiMaio, A. Deguet, B. Vagvolgyi, M. Balicki, C. Schneider, R. Kumar, A. Jog, B. Itkowitz, C. Hasser, and R. Taylor, "The Surgical Assistant Workstation (SAW) in minimally-invasive surgery and microsurgery," *Midas Journal*, Jun 2010. [Online]. Available: http://hdl.handle.net/10380/3179

[8] S. D. Pieper, M. Halle, and R. Kikinis, "3D Slicer," in *IEEE Intl. Symp. on Biomedical Imaging (ISBI)*, Apr 2004, pp. 632–635.

[9] J. Tokuda, G. S. Fischer, X. Papademetris, Z. Yaniv, L. Ibanez, P. Cheng, H. Liu, J. Blevins, J. Arata, A. J. Golby, T. Kapur, S. Pieper, E. C. Burdette, G. Fichtinger, C. M. Tempany, and N. Hata, "OpenIGTLink: an open network protocol for image-guided therapy environment," *Intl. J. of Medical Robotics and Computer Assisted Surgery*, vol. 5, no. 4, pp. 423–434, 2009.

[10] P. J. Stolka, H. J. Kang, and E. Boctor, "The MUSiiC toolkit: modular real-time toolkit for advanced ultrasound research," *MIDAS Journal*, Jul 2010. [Online]. Available: http://hdl.handle.net/10380/3172

[11] H. J. Kang, P. J. Stolka, and E. Boctor, "OpenITGLinkMUSiiC: a standard communications protocol for advanced ultrasound research," *MIDAS Journal*, Jul 2011. [Online]. Available: http://hdl.handle.net/10380/3301

[12] L. Mo, D. DeBusschere, G. McLaughlin, D. Napolitano, W. Bai, K. Fowkes, A. Irish, X. Wang, J. B. Fowlkes, and P. L. Carson, "Compact ultrasound scanner with simultaneous parallel channel data acquisition capabilities," in *Proc. IEEE Intl. Ultrasonics Symp.*, Nov 2008, pp. 1342–1345.